AIAA SciTech Forum
23-27 January 2023, National Harbor, MD & Online
AIAA SCITECH 2023 Forum

10.2514/6.2023-0463

Aerodynamic Forces and Wake Analysis of Wing Damaged Flapping Flight

Alec Menzer[1], Haibo Dong[2]
Department of Mechanical and Aerospace Engineering, University of Virginia, Charlottesville, VA 22903, USA

Flapping flight is a commonly used mechanism of micro aerial vehicles and insects alike. Dragonflies use their four-winged anatomy to navigate the environment, maneuver around obstacles, and perform other essential flight patterns. The flight performance and aerodynamics of intact flapping wings is well known; however, this study aims to clarify how wing damage affects the flight performance. First, high speed videos of the damaged wing flight, a takeoff performed by a dragonfly, is captured, and subsequently digitally reconstructed to create a three-dimensional model. Second, using an immersed-boundary method (IBM) based incompressible Navier-Stokes direct numerical simulation (DNS) solver, we resolve the aerodynamic forces and wake topology of the dragonfly's damaged wing flapping flight in high detail. We found that spanwise damage doesn't cause any detriment to the force capabilities of the damaged wing which is due to increased pitch angles of the damaged wing. As a consequence, fliers with spanwise damaged and intact wings may be able to utilize similar strategies to achieve takeoffs. The wake topology of the wing damaged flight is also examined. This work serves as a baseline for studying the effect of wing damage for flapping flight and could provide useful insights to micro-aerial vehicle (MAV) designers as some degree of wing damage may be an inevitable occurrence for winged fliers.

I. Nomenclature

θ_w, Ψ_w, Φ_w	=	wing deviation, stroke, and pitch angle
θ_b, Φ_b, Ψ_b	=	body pitch, yaw and roll Euler angles
f	=	flapping frequency
s	=	span length
c	=	undamaged chord length
S	=	average undamaged wing area
AR	=	aspect ratio
C_A	=	normalized coefficient of variable 'A'
$A, \bar{A}$	=	time varying and time averaged value of variable 'A'
O-XYZ	=	global coordinate system
O-$X'Y'Z'$	=	body local coordinate system
Re	=	Reynolds number
U_{tip}	=	wing tip velocity
ω_s	=	spanwise vorticity

II. Introduction

Wing wear is common among flying taxa and can be cumulative and irreversible, often resulting from external damage [1]. Non-repairable damage of insect wings, a problem that micro aerial vehicles (MAVs) may also face, is

[1] Ph.D. Student, dfg5nb@virginia.edu
[2] Professor, haibo.dong@virginia.edu, AIAA Associate Fellow

linked repeated collision with stationary environmental obstacles, for example [2]. As such, we aim to learn from an insect's capability of wing-damage flight for application to flapping MAV design. Although insects with damaged wings can still fly [1], flight performance may be compromised because of the wing area reduction, which inevitably will affect the flight forces.

Several studies have investigated the consequences of wing damage on flight behavior with the majority being focused on two winged fliers such as flies [3], functionally four-winged fliers like hawkmoths [4], and also four-winged fliers like Odonates [1],[5]. For the current study, we choose to analyze dragonflies (Odonate) as many MAV platforms have taken inspiration from their wing shape and flight [6-8]. Regarding dragonflies, a recent work [2] showed that typical area loss of collected specimen was <10% while severe damage was as much as 75%. Critical zones of wing damage were concentrated at the distal part of the wings toward to the trailing edge for both wing pairs and around the proximal part of the hindwings (near the wing base) toward the trailing edge. It is generally understood that, to compensate for wing damage, insects rely on adjustments of both the wing and body kinematics such as increased flapping frequency, flapping amplitude, reduction in vertical acceleration, stoke plane angle adjustment, changes in wing rotation timing, and adjustment of body roll to damaged side [3,4,9].

However, minimal understanding of the aerodynamic mechanisms behind wing damaged flight exists. Studies do address aerodynamic features of insect-like flapping flight [10-12]. For Odonate flight, which will be examined in this study, detailed computational work has characterized aerodynamic features of many other intact wing flight modes though. For example, in takeoff flight of a damselfly, the wing upstrokes are generally aerodynamically more active compared to the downstroke (DS) due to the body position, speed and angle of attack [13] whereas the DS is more active in forward flight [14]. Similarly, during a dragonfly's backwards flight, role reversal is clear in which the upstroke (US) becomes more aerodynamically active than the downstroke (DS) due to body reorientation strategies [15]. In turning flight, vertical force generation is split 64/36 between the forewings/hindwings (with clear DS favorability) and the forewings were also primary horizontal force contributors too. Also, wing-wing interaction led to lower power consumption and enhanced force production [16], which has also been shown to occur for canonical ipsilateral flapping motions too [17].

There exists a clear gap in our understanding of wing damaged flight, and important questions regarding the aerodynamic roles of the flaps as well as the corresponding effect on the wake topology remain unanswered despite their importance in a comprehensive understanding of flapping flight and even designing MAVs robust to wing area loss. This study aims to bridge this gap by combining experimental and computational techniques to record and reconstruct wing damaged dragonfly flight and subsequently use perform CFD simulations on the model. Doing so, a better understanding of wing damage and its effects on flapping flight can be obtained. Methods are presented in Sec. III, followed by detailed aerodynamic results in Sec. IV. Summarizing statements are made in Sec. V.

III. Methodology

A. Reconstruction and Kinematics

We captured dragonflies (*Erythemis simplicicollis*) with undamaged wings and transported them to the laboratory for experiments. The wings were marked and incised, performing a spanwise cut on the left forewing (LF) using a pair of household scissors. This cut removed 40% of the wing area at the trailing edge which has previously been identified as a common region of wing area loss [1]. Afterwards, we recorded various flights using a high-speed videography setup. Footage in which the dragonfly performed a left-banked takeoff was chosen for analysis, as it is expected the upwards acceleration period will contain rich information on both the aerodynamic forces and wake topology. To create the digital models for simulation, a point-based reconstruction of the video footage was performed [18,19], using Autodesk Maya. A comparison of the real dragonfly and computational model Fig. 1a,b (respectively) as well as clarification of the global and body reference frame in Fig. 1b. We note that the body (shown in a lighter grey shade in Fig. 1b) is reconstructed for analysis of the body motion but is not included in the CFD simulation to simplify the computations.

We tabulate some of the body and wing kinematics characteristics in Table 1. More detailed descriptions of the kinematic definitions used in the paper can be found in ref. [13]. The dragonfly executes a liftoff and banked left turn during a 160ms time window. During the maneuver period, the dragonfly translates 1.90L upwards (in Y direction) and 2.20L horizontally (in the XZ plane). Additionally, the heading angle progresses through a 120˚ counterclockwise

(CCW) rotation (w.r.t. global frame), hence, the damaged LFW is on the weak side of the turn. We also compare some basic wing kinematics for the model, too. Primarily, we examine the FWs, since neither of the hindwings are damaged. The stroke amplitude and deviation amplitude seem relatively close between the damaged and undamaged FWs. Meanwhile, the average pitch angle is quite different, with the damaged LF maintaining a 10˚ higher pitch angle on average. We note that the pitching angle discrepancies are dominantly in the US too, with the instantaneous LF pitch angle reaching up to 36˚ larger than the RF during the 2nd US.

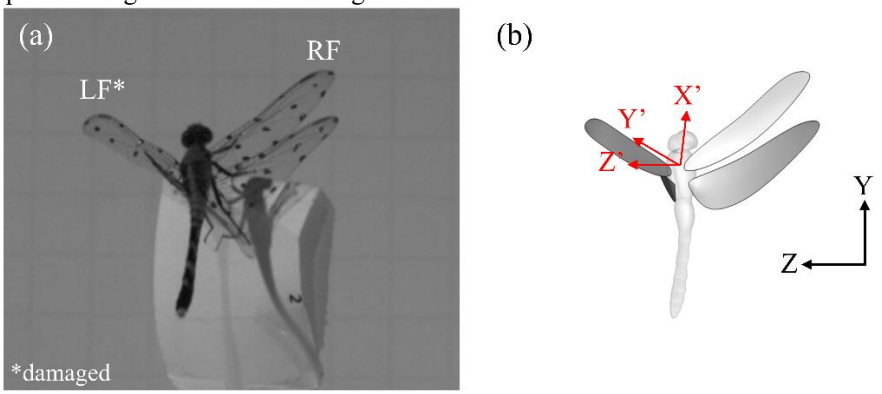

Figure 1: Comparison of the dragonfly; (a) capture on video and; (b) reconstructed computational model, with indication of body frame axes with X' pointed forward, Y' pointed laterally, and Z' pointed vertically relative to the body

Table 1: Body and wing kinematic characteristics describing the motion of the wing damaged dragonfly (* damaged)

Duration (ms)	Vert. Disp. (L)	Horz. Disp. (L)	Heading Disp. (˚)	Ψ_w Amp. (˚)		θ_w Amp. (˚)		$\bar{\Phi}_w$ (˚)	
				LF	RF	LF	RF	LF	RF
160	1.90	2.20	120	80*	85	12*	14	98*	87

B. Governing equations, numerical method, and simulation setup

The governing equations solved in this work are the incompressible Navier-Stokes equations, written in indicial form in equation 1.

$$\frac{\partial u_i}{\partial x_i} = 0; \quad \frac{\partial u_i}{\partial t} + \frac{\partial u_i u_j}{\partial x_j} = -\frac{\partial p}{\partial x_i} + \frac{1}{Re}\frac{\partial^2 u_i}{\partial x_i \partial x_j} \qquad \text{Eqs. (1)}$$

where u_i are the velocity components, p is the pressure and Re is the Reynolds number ($Re = \frac{\bar{U}_{ref}\,\bar{c}}{\upsilon}$, where $\bar{c}$ is the average undamaged chord length, $\bar{U}_{ref}$ is the average reference velocity and υ is the kinematic viscosity). The Re selected for this study is 1600. The velocity and pressure variables in Eq. (1) are nondimensionalized with the appropriate time and length scales.

To solve these equations an in-house finite-difference based Cartesian-grid sharp-interface immersed-boundary method direct numerical simulation solver (DNS) is employed. The DNS used in this study employed a second order fractional time step method for temporal discretization. To retain second order spatial accuracy, convective terms in Eq. (1) are discretized using an Adams–Bashforth and diffusive are discretized using an implicit Crank–Nicolson scheme. In depth information regarding this solver can be found in ref. [20]. Recent applications of the solver used in the current study for flapping kinematics include manta flapping, hummingbird flight, damselfly gliding flight, and fruit fly flight [21-25]. A graphic of the computational domain signifying the boundary conditions and wing flapping motion in the fluid domain is shown in Figure 2. The domain measures 288 × 256 × 288 grids with a minimum grid spacing of Δ=0.0125 immediately surrounding the wings.

To describe the aerodynamic forces and power consumption C_V, C_H are used. Forces are computed by integrating the pressure and shear forces across each of the wings. The aerodynamic forces are resolved into horizontal (H) and vertical (V) components, with V computed to be force in the +Y direction and H as the force magnitude in the XY plane opposite to the heading direction. Forces are non-dimensionalized according to Eq. (2).

$$C_{V,H} = \frac{V,H}{\frac{1}{2}\rho {U_{tip}}^2 S} \tag{2}$$

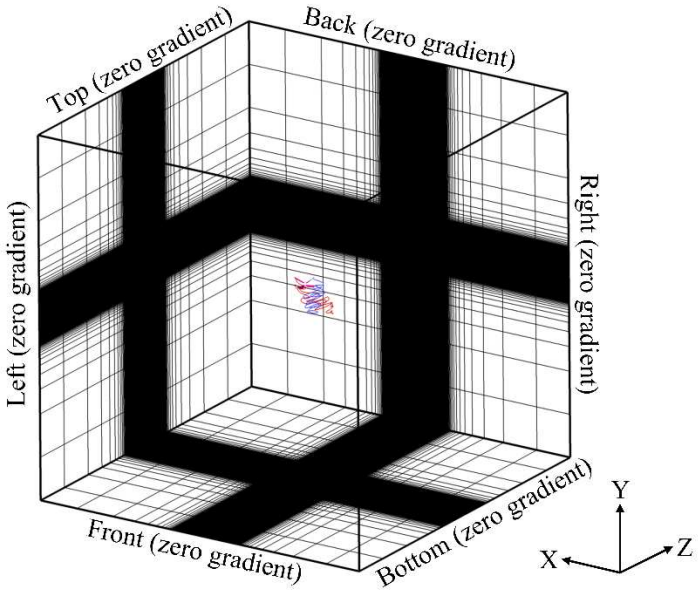

Figure 2: Computational domain with boundary conditions indicated, as well as the wings (pink) and LF/H and RF/H trajectories (red and blue, respectively).

IV. Results and Discussion

Next, we analyze the aerodynamic forces produced by the wings to clarify any changes in the aerodynamic roles that arise due to spanwise area loss. Finally, the three-dimensional wake topology and surfaces pressures are analyzed to correlate vortex formation to the observed aerodynamic force patterns.

A. A Global and Local Analysis of Aerodynamic Forces

In this section, we analyze aerodynamic performance to determine to what extent spanwise wing damage affects force generation. To start, we show the time history of the dragonflies C_V, C_H (which are defined in a global sense) for each of the wigs in Fig. 3. The DS period is denoted by a grey background and US by a white background.

Some intriguing patterns arise from inspection of the time series data. Firstly, we will focus on the FW US for both the left and right sides as they play a large role in the C_V production during the 1st two strokes. This is evident in the large peaks in lift after the half-US time (white background) during stroke I and II. As for the HWs, less consistent US or DS bias towards vertical force is observed in the beginning, however, towards the end of the captured motion the HWs do seem to favor C_V during the DS. This characteristic of US favored vertical force production, as seen at the start of the motion, is a feature of wing damaged flapping flight takeoff flight not yet documented and indicates that spanwise area loss on one of the FWs does not have serious weight-support consequences. With regards to the horizontal force, we observe that the HWs are more dominantly C_H producing compared to the FWs with overall larger magnitude C_H generated by the HWs.

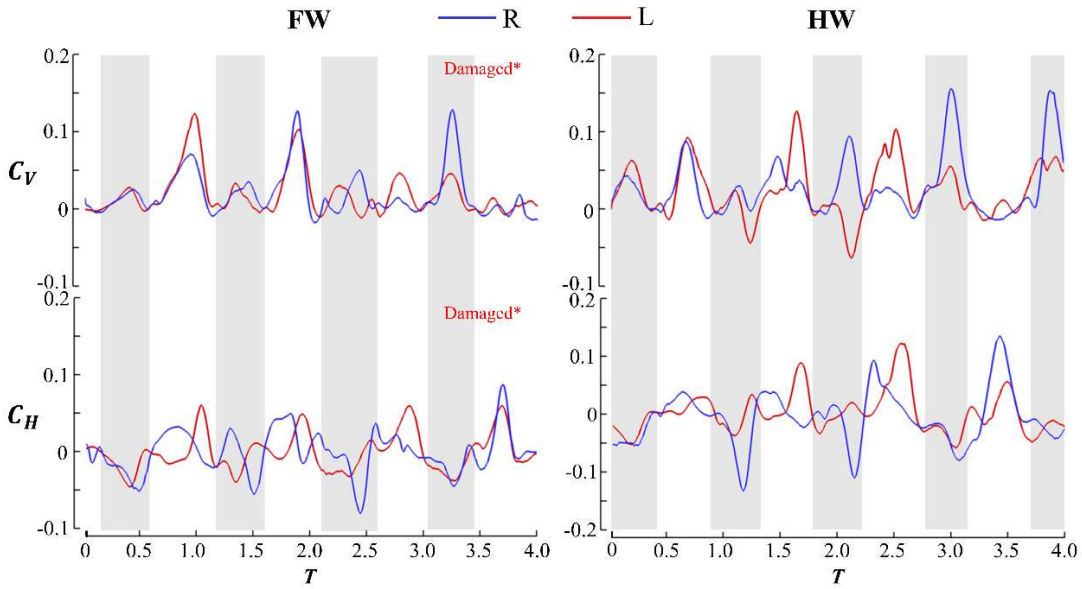

Figure 3: Global force history for the FWs and HWs, with indication of US (white) and DS (grey) given via background coloring.

To gain a more complete understanding of the wing damaged aerodynamic force generation, we examine the forces relative to the local body frame in Fig. 4. In the global frame, we identified that the spanwise wing damage does not seem to have any weight support consequences during the 1st two strokes in which the takeoff occurs. Now, we shift our focus to the local frame to identify how this weight supporting force is achieved. Locally, we define force coefficients along the X' and $-Z'$ axis (Fig. 1) as $C_{H'}$ and $C_{V'}$ which follow similar definitions to Eq. (2). A time series of this data is plotted in Fig. 4, and we select two time instances in which to illustrate the body position: T=1.42 (mid 2nd FW DS) and T=1.94 (mid 2nd FW US). The local force orientation is also shown to help visualize the relationship between the local and global frame forces.

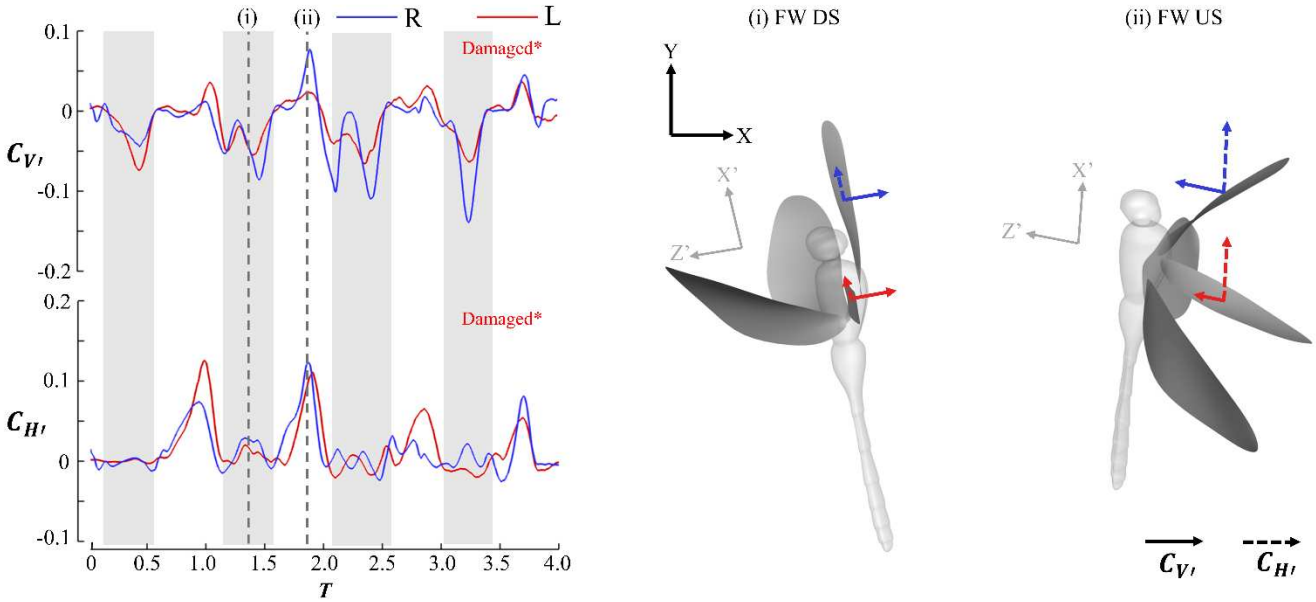

Figure 4: Comparison of aerodynamic forces in the body local frame shown as a time series and also with the local vertical and horizontal forces projected onto the wing mid-span at; (i) the mid-DS and; (ii) the mid-US of the 2nd stroke. The arrows at the bottom left indicate a relative size of 0.1.

Force vectoring, documented previously for flapping flight with all intact wings [13] but not yet with damaged wings, is clear from the relationship to between local frame $C_{V'}$ / global frame C_H and local frame $C_{H'}$ / global frame C_V. During the 2nd FW US, the relatively small global C_V production matches low $C_{H'}$ production. Correspondingly, during the 2nd FW DS, the large peaks in C_V (Fig. 3) correspond exactly to the high $C_{H'}$ (Fig. 4). During the US, the local frame $C_{H'}$ is dominant which also aligns well with the prominence of global frame C_V at the same time. This reorientation of flight forces in the global frame is due to the steep body posture which is clarified in Fig. 4(i,ii). The large body frame horizontal forces produced by both the intact RF and damaged LF during the US are predominantly responsible for the large global frame forces seen in Fig. 3. This also occurs for intact wing flapping flight takeoff [13] so we find that despite having spanwise wing damage, non-steady flight patterns such as a takeoff can still be achieved using similar strategies as with intact wings.

B. Wake topology and surface pressure

To accompany the aerodynamic force calculations computed previously, we analyze the 3-D wake topology using iso-surfaces defined characterized by Q-criterion values of 100. The primary focus of the flow analysis is to examine the vortex formation of the damaged and intact LF and RF, respectively. The 2nd flapping motion is selected as a representative stroke to match the discussion of forces made for the mid-DS and mid-US in the previous section.

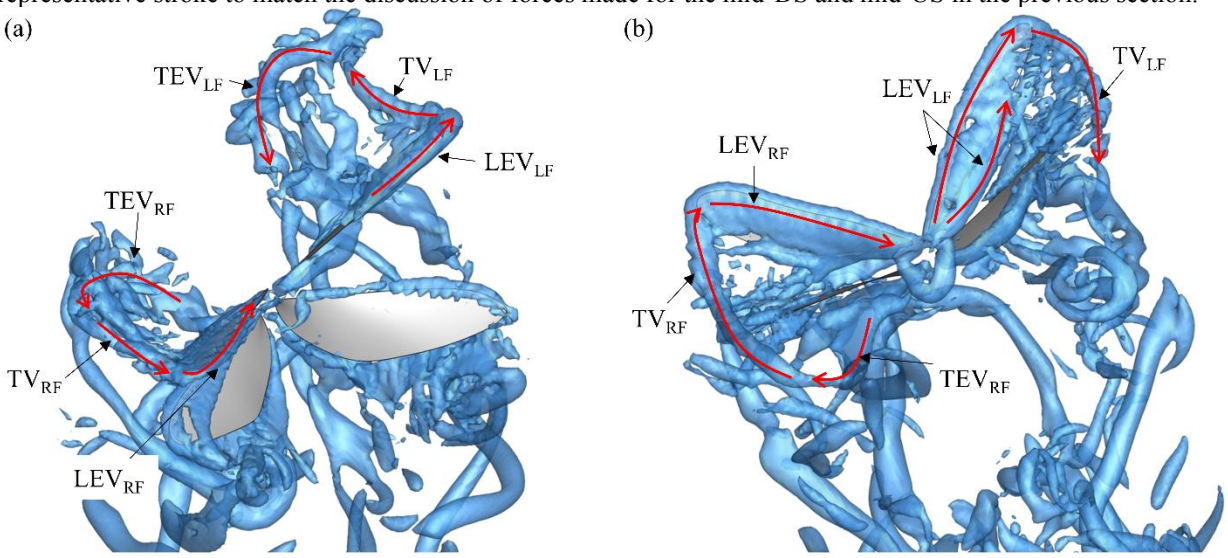

Figure 5: Q-criterion visualization for the; (a) mid-DS and; (b) mid-US

At the mid-L/RF DS, shown in Fig. 5a., distinct leading-edge vortex (LEV), tip vortex (TV) and rings (R) are clear. Some small differences can be observed for the LEV, with the LEV$_{LF}$ predominantly forming on the distal regions of the wing and exhibits some characteristics of flow separation onset (evident from the less-flattened profile). The LEV$_{RF}$ is present along a larger portion of the leading edge and has a more flattened profile, indicating attachment to the wing. Vortex rings, formed by interconnection of shed trailing-edge vortexes (TEVs), LEVs, and TVs, are also clear behind the wing and are alike in size for both the damaged LF and intact RF. Progressing to the mid-US, the cause for huge global vertical force production (Fig. 3) for both FWs is clear. Each FW forms LEVs along a large portion of the wing leading edge. We do notice some interesting behavior of the LEV$_{FW}$, though, as it appears to have a primary and secondary structure. Regardless, LEVs on both wings are both relatively similar in size during the US and are the primary mechanism the flapping wings can produce aerodynamic forces. No TEV is visible in the wake of the LF whereas the RF does exhibit TEV$_{RF}$ formation.

To supplement the Q-criterion information, we also give a more detailed illustration of the FW LEV formation in Fig. 6 through spanwise slice cuts and surface pressure information in Fig. 7. Spanwise cuts are made by calculating the flow information in planes perpendicular to the root-tip vector, as if a virtual camera was viewing directly down the span. The spanwise vorticity, ω_S, is normalized by $\bar{U}_{tip}\bar{c}$. The time instances shown correspond to those shown in Fig. 5(a) and Fig. 4(i) for the DS and Fig. 5(b) and Fig. 4(ii) for the US. At the mid-DS, shown in Fig. 6(a,b), the slight differences in LEV attachment between the LF and RF is confirmed. The LEV$_{RF}$ is flatter to the wing and is present closer to the wing root while the LEV$_{LF}$ demonstrates separation but a seemingly stronger core farther along the span (indicated by the denser spanwise vorticity contour). During the US, shown in Fig. 6(c,d) the mid-US time is shown.

The LEV spanwise vorticity regions are much stronger for the US than for the DS for both the LF and RF which can be seen by comparing the size and density of the dark vorticity contour regions. We also observe the secondary LEV_{LF}' structure that has not occurred on the RF. The spanwise area loss near the trailing edge may also have some impact on wing-wing interactions, after all, TEVs shed from the smaller LF are further in proximity to the leading edge of the LH. Meanwhile, the TEVs shed from the RF are closer to the RW. Due to this, no interaction between the LF and LW is observed during the US, meanwhile, there is some interaction between the RF and RW indicated by the red-circled region.

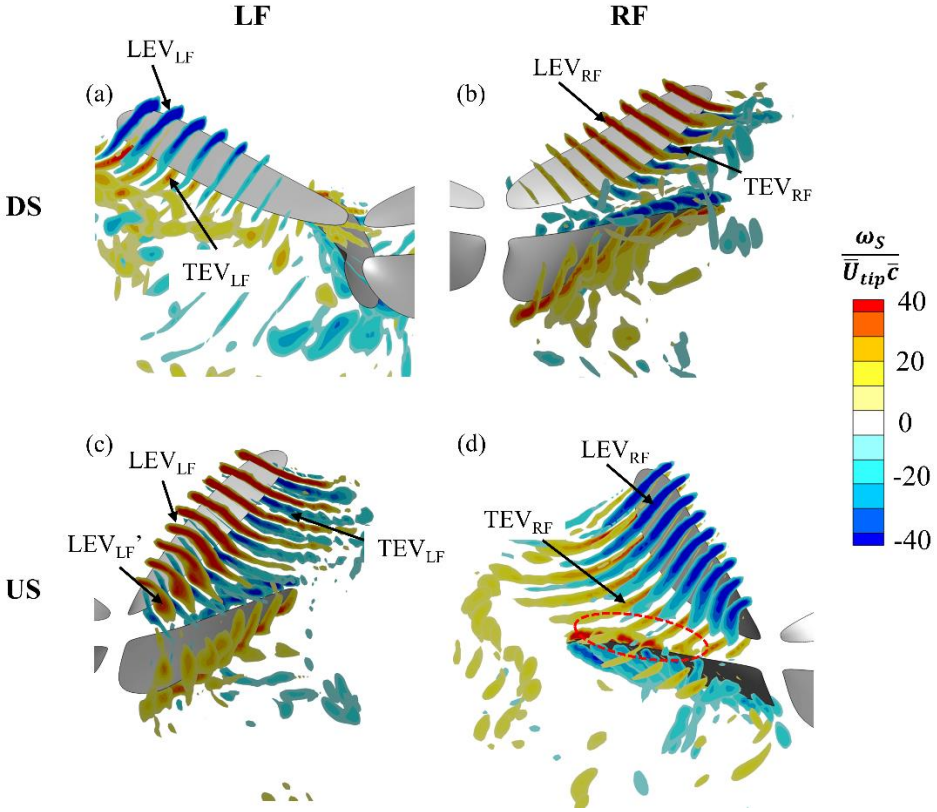

Figure 6: Spanwise vorticity contours shown for the; (a,c) LF and; (b,d) RF at the mid-DS (a,b) and mid-US (c,d).

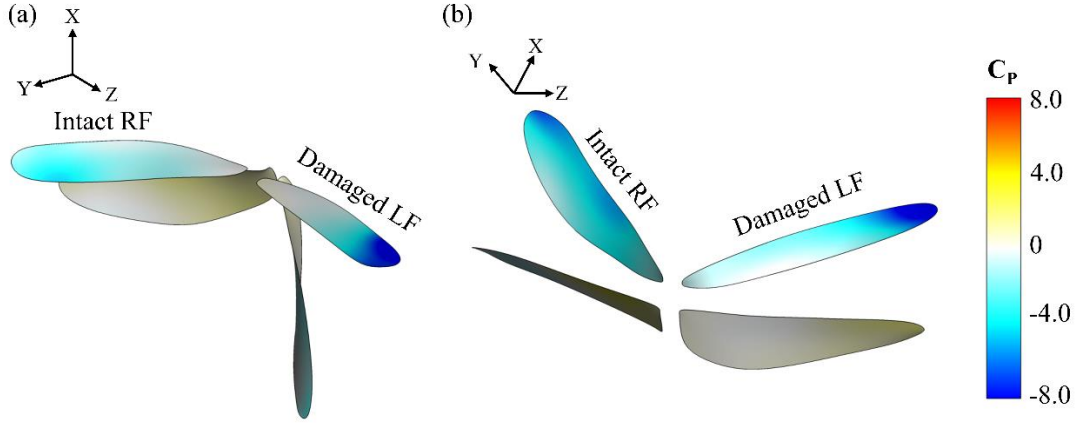

Figure 7: Surface pressure differential distribution at the mid-DS (a) and mid-US (b).

Corresponding to the spanwise circulation, we plot the surface pressure differential (between the top and bottom surfaces) distribution in Fig. 6. We can clearly see that the damaged LF is able to produce larger low-pressure regions (indicated by large dark blue regions) at the outer regions of the wing to compensate for the area loss at the trailing

edge where the intact RF can still generate aerodynamic forces. These regions of large pressure gradients agree well with the locations of the formed LEVs, which help to generate pressure differentials, and is also consistent with the observation from Sec. III that the LF pitch angle is overall larger than the RF, especially in the US as larger pitch angles do in general lead to more aerodynamic forces at the distal wing regions [26].

V. Conclusions

In this study, the effect of wing damage on flapping flight is investigated through experimental video capture of a dragonfly with spanwise area loss and an associated high-fidelity fluids simulation. Previous works have addressed some behaviors associated with wing damage; however, we characterized the aerodynamics and wake topology to better understand spanwise area loss effects. Prominently, we found that sufficient weight-supporting forces can still be generated by the damaged wing. This weight support is achieved by reorienting the body forces via body posture, a characteristic of wing damaged flapping flight unstudied previously. We also analyzed the wake topology. The damaged LF still produces strong LEVs and can even induce large surface pressure gradients to compensate for the lower wing area, which explains the similarities in force production during the first two flapping strokes. Increased pitching angles on the spanwise damaged side lead to the observed flight force patterns. Specifically, the damaged LF wing pitch is consistently higher than the intact RF, especially in the 2nd stroke, and correspondingly the flight forces are nearly the same between the two wings despite the lower LF wing area.

Future work make include different types of wing damage, after all, area loss at different parts of the wing damage may impact the force production capability of flapping flight differently. Additionally, our simulations indicate that spanwise wing damage does impact wing-wing interaction between the trailing edge of the damaged FW and leading edge of the HW. We only analyzed one type of wing damage during takeoff flight and further analysis of other wing damage types during other flight patterns is required to determine whether wing-wing interaction is still possible with wing damage.

Acknowledgments

A thanks goes out to Ayodeji Bode-Oke and Kuo Gai for their work on the original wing damaged dragonfly reconstruction. Additionally, thank you to University of Virginia's Research Computing group for the availability of the Rivanna supercomputing cluster. This work was supported by NSF CEBT-1313217, NSF CNS-1931929 and the NSF NRT Grant No. 1829004.

References

[1] Rajabi, H., Schroeter, V., Eshghi, S., and Gorb, S. N. "The Probability of Wing Damage in the Dragonfly Sympetrum Vulgatum (Anisoptera: Libellulidae): A Field Study." *Biology Open*, Vol. 6, No. 9, 2017, pp. 1290–1293. https://doi.org/10.1242/bio.027078.

[2] Foster, D. J., and Cartar, R. V. "What Causes Wing Wear in Foraging Bumble Bees?" *Journal of Experimental Biology*, Vol. 214, No. 11, 2011, pp. 1896–1901. https://doi.org/10.1242/jeb.051730.

[3] Muijres, F. T., Iwasaki, N. A., Elzinga, M. J., Melis, J. M., and Dickinson, M. H. "Flies Compensate for Unilateral Wing Damage through Modular Adjustments of Wing and Body Kinematics." *Interface Focus*, Vol. 7, No. 1, 2017. https://doi.org/10.1098/rsfs.2016.0103.

[4] Fernández, M. J., Driver, M. E., and Hedrick, T. L. "Asymmetry Costs: Effects of Wing Damage on Hovering Flight Performance in the Hawkmoth Manduca Sexta." *Journal of Experimental Biology*, Vol. 220, No. 20, 2017, pp. 3649–3656. https://doi.org/10.1242/jeb.153494.

[5] Combes, S. A., Crall, J. D., and Mukherjee, S. "Dynamics of Animal Movement in an Ecological Context: Dragonfly Wing Damage Reduces Flight Performance and Predation Success." *Biology Letters*, Vol. 6, No. 3, 2010, pp. 426–429. https://doi.org/10.1098/rsbl.2009.0915.

[6] Kok, J. M., and Chahl, J. S. "Design and Manufacture of a Self-Learning Flapping Wing-Actuation System for a Dragonfly-Inspired MAV." *54th AIAA Aerospace Sciences Meeting*, AIAA, 2016. https://doi.org/10.2514/6.2016-1744.

[7] Hu, Z., Mccauley, R., Schaeffer, S., and Deng, X. "Aerodynamics of Dragonfly Flight and Robotic Design." *Proceedings of the IEEE International Conference on Robotics and Automation*, IEEE, 2009. https://doi.org/10.1109/ROBOT.2009.5152760.

[8] Jang, J. H., and Yang, G. H. "Design of Wing Root Rotation Mechanism for Dragonfly-Inspired Micro Air Vehicle." *Applied Sciences*, Vol. 8, No. 10, 2018, pp. 10–12. https://doi.org/10.3390/app8101868.

[9] Fernández, M. J., Springthorpe, D., and Hedrick, T. L. "Neuromuscular and Biomechanical Compensation for Wing Asymmetry in Insect Hovering Flight." *Journal of Experimental Biology*, Vol. 215, No. 20, 2012, pp. 3631–3638. https://doi.org/10.1242/jeb.073627.

[10] Dong, H., Liang, Z., and Harff, M. "Optimal Settings of Aerodynamic Performance Parameters in Hovering Flight." *International Journal of Micro Aerial Vehicles*, Vol. 1, No. 3, 2009. https://doi.org /10.1260/175682909789996195.

[11] Geng, B., Xue, Q., Zheng, X., Liu, G., Ren, Y., and Dong, H. "The Effect of Wing Flexibility on Sound Generation of Flapping Wings." *Bioinspiration and Biomimetics*, Vol. 13, No. 1, 2018. https://doi.org/10.1088/1748-3190/aa8447.

[12] Wan, H., Dong, H., Huang, G.P. "Hovering Hing-Connected Flapping Plate with Passive Deflection" *AIAA Journal*, Vol. 50, No. 9, 2012, pp. 2020-2026. https://doi.org/10.2514/1.J051375.

[13] Bode-Oke, A. T., Zeyghami, S., and Dong, H. "Aerodynamics and Flow Features of a Damselfly in Takeoff Flight." *Bioinspiration and Biomimetics*, Vol. 12, No. 5, 2017. https://doi.org/10.1088/1748-3190/aa7f52.

[14] Sato, M., and Azuma, A. "The Flight Performance of a Damselfly Ceriagrion Melanurum Selys." *Journal of Experimental Biology*, Vol. 200, No. 12, 1997, pp. 1765–1779. https://doi.org/10.1242/jeb.200.12.1765.

[15] Bode-Oke, A. T., Zeyghami, S., and Dong, H. "Flying in Reverse: Kinematics and Aerodynamics of a Dragonfly in Backward Free Flight." *Journal of the Royal Society Interface*, Vol. 15, No. 143, 2018. https://doi.org/10.1098/rsif.2018.0102.

[16] Li, C., and Dong, H. "Wing Kinematics Measurement and Aerodynamics of a Dragonfly in Turning Flight." *Bioinspiration and Biomimetics*, Vol. 12, No. 2, 2017. https://doi.org/10.1088/1748-3190/aa5761.

[17] Dong, H., Liang, Z. "Effects of Ipsilateral Wing-Wing Interactions on Aerodynamic Performance of Flapping Wings." *48th AIAA Aerospace Sciences Meeting*, AIAA, 2010. https://doi.org/10.2514/6.2010-71.

[18] Koehler, C., Liang, Z., Gaston, Z., Wan, H., and Dong, H. "3D Reconstruction and Analysis of Wing Deformation in Free-Flying Dragonflies." *Journal of Experimental Biology*, Vol. 215, No. 17, 2012, pp. 3018–3027. https://doi.org/10.1242/jeb.069005.

[19] Dong, H., Koehler, C., Liang, Z., Wan, H., and Gaston, Z. "An Integrated Analysis of a Dragonfly in Free Flight." *28th AIAA Applied Aerodynamics Conference*, AIAA, Vol. 1, 2010. https://doi.org/10.2514/6.2010-4390.

[20] Mittal, R., Dong, H., Bozkurttas, M., Najjar, F. M., Vargas, A., and von Loebbecke, A. "A Versatile Sharp Interface Immersed Boundary Method for Incompressible Flows with Complex Boundaries." *Journal of Computational Physics*, Vol. 227, No. 10, 2008, pp. 4825–4852. https://doi.org/10.1016/j.jcp.2008.01.028.

[21] Menzer, A., Li, C., Fish, F., Gong, Y., Dong, H. "Modeling and Computation of Batoid Swimming Inspired Pitching Impact on Wake Structure and Hydrodynamic Performance." *Proceedings of the ASME Fluids Engineering Division Summer Meeting,* ASME, 2022. https://doi.org/10.1115/FEDSM2022-86684.

[22] Menzer, A., Ren, Y., Guo, J., Tobalske, B. W., and Dong, H. "Wing Kinematics and Unsteady Aerodynamics of a Hummingbird Pure Yawing Maneuver." *Biomimetics*, Vol. 7, No. 3, 2022, p. 115. https://doi.org/10.3390/biomimetics7030115.

[23] Ren, Y., Dong, H., Deng, X., and Tobalske, B. "Turning on a Dime – Asymmetric Vortex Formation in Hummingbird Maneuvering Flight". *Physical Review Fluids,* Vol. 1, No. 050511, 2016. https://doi.org/10.1103/PhysRevFluids.1.050.511.

[24] Pan, Y., Zhang, Z., and Dong, H. "Computational Study on Gliding Flight of a Damselfly." *AIAA SciTech Forum*, AIAA, 2022. https://doi.org/10.2514/6.2022-0728.

[25] Li, C., Dong, H., and Zhao, K. "A Balance between Aerodynamic and Olfactory Performance during Flight in Drosophila." *Nature Communications*, Vol. 9, No. 1, 2018, pp. 1–8. https://doi.org/10.1038/s41467-018-05708-1.

[26] Li, C., and Dong, H. "Wake Structure and Aerodynamic Performance of Low Aspect-Ratio Revolving Plates at Low Reynolds Number." *52nd Aerospace Sciences Meeting*, AIAA, 2014. https://doi.org/10.2514/6.2014-1453.